Presented at HIPAGS'93
Massachusetts Institute of Technology
January 13-15, 1993

BNL-48587

GLOBAL TRANSVERSE AND FORWARD ENERGY MEASUREMENTS FOR Si+A AND Au+A AT THE AGS

BRUCE MOSKOWITZ
Department of Physics
Brookhaven National Laboratory, Upton, NY 11973, USA

for the E802/866 Collaboration:
ANL-BNL-UCB-UCR-Columbia-Hiroshima-INS-
Kyushu-LLNL-MIT-NYU-Tokyo-Tsukuba

ABSTRACT

The global transverse and forward energy from Si+Al,Au at 14.6A GeV/c and Au+Al,Au at 11.6A GeV/c have been measured using the E802 lead-glass and ZCAL. Preliminary $d\sigma/dE_T$, $dE_T/d\eta$ and $d\sigma/dT_{ZCAL}$ spectra are presented, and the shapes of the spectra from different systems are compared. The transverse and forward energies in Au+Au are observed to be anticorrelated in a manner that is reproduced by the cascade model ARC but not by the essentially geometric model Fritiof.

1. Introduction

The flow of energy from the beam (forward energy) into the midrapidity region (transverse energy) reveals much of the large-scale character of relativistic heavy ion collisions. The E802 Collaboration has previously reported results[1,2] on this topic from measurements with the AGS silicon beam using a beam calorimeter and a lead-glass array. With the recent arrival of the gold beam, a new set of measurements was performed in order to systematically compare the projectile dependence from Si to Au.

2. The Experimental Apparatus

A set of calorimetry measurements was performed in April 1992 with both the 14.6A GeV/c ^{28}Si and the new 11.6A GeV/c ^{197}Au beams. For these runs, the E802 magnetic spectrometer was moved as far away as possible from the beam and a new array of 64 lead-glass blocks was inserted 1.5 m downstream of the target. The new array was on the opposite side of the beam from the existing E802 lead-glass array of 245 blocks which was 3.0 m downstream of the target.[2] For all the results reported, a fiducial cut was applied such that the solid angle coverage of both arrays was identical, and that almost all blocks inside the fiducial region were completely surrounded by other blocks, thus minimizing leakage effects, etc. The coverage of the fiducial region is $1.3 \leq \eta \leq 2.4$ and $0 \leq \phi < 2\pi$. The lead-glass responds mainly to electromagnetic energy, but there is also a significant contribution from the Čerenkov radiation of charged hadrons above threshold; it is estimated that 95% of the total signal

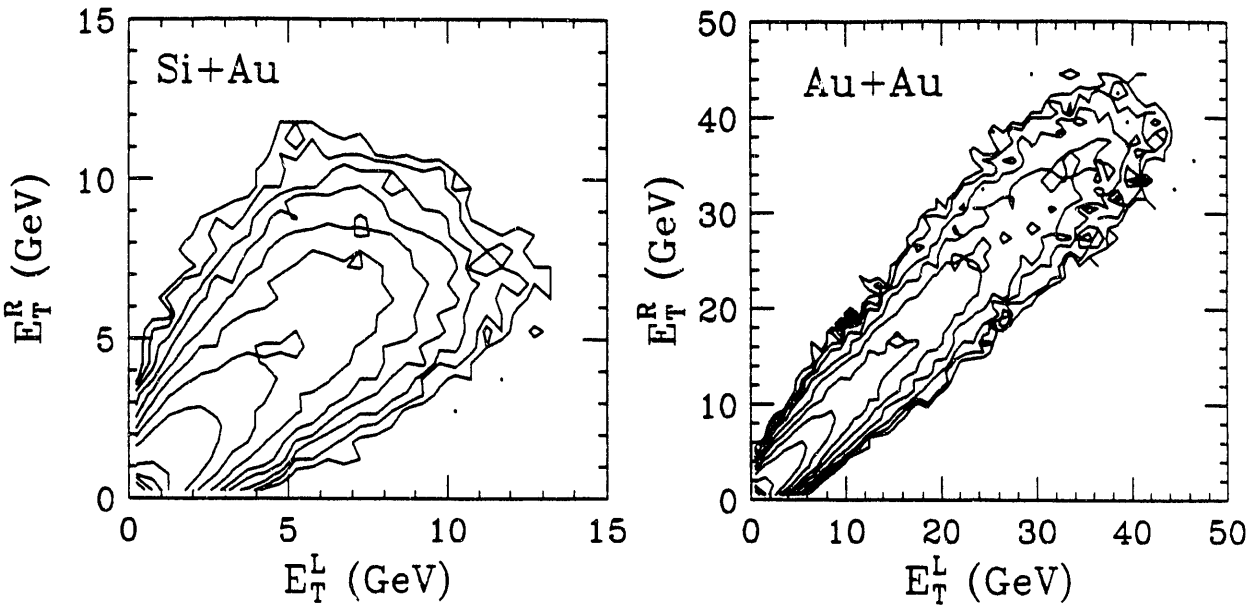

Fig. 1: Correlation of the transverse energy as measured in the left detector versus that measured in the right detector for minimum bias Si+Au and Au+Au events. The contour lines are logarithmic with a factor of two difference between adjacent lines.

for Si+Au reactions is due to *produced* particles[4]. For more details on the response and calibration of the lead-glass see Refs. 2 and 3.

Forward energy was detected in the E802 Zero-degree Calorimeter (ZCAL)[5] which covered angles $\theta \geq 1.5°$ and essentially counted the number of projectile spectator nucleons.

3. Left and Right Transverse Energy

Fig. 1 shows the correlation between the transverse energy measured in the "left" detector (the new 64 block array) and that in the "right" detector (the 249 block array.) These quantities are defined by:

$$E_T^{L\ (R)} = \sum_{L\ (R)} E_i \sin\theta_i \quad , \tag{1}$$

where E_i is the energy in block i, θ_i is the polar angle from the beam axis to the center of the face of block i, and the sum is over all blocks, i, in the fiducial acceptance of the left (right) array for which $E_i \geq 200$ MeV. Note that the ridge line in both plots of Fig. 1 forms a 45° angle with respect to the E_T^L and E_T^R axes, demonstrating that the two detectors are well balanced in response. The two quantities are especially correlated in the case of Au+Au.

4. Global Transverse Energy Spectra

The left and right detectors were combined to find the total transverse energy:

$$E_T^{L+R} = E_T^L + E_T^R \quad . \tag{2}$$

system	E_T^{L+R} cut (GeV)	ρ (GeV)	η_{peak}	σ_{rms}	χ^2/d.o.f.
Si+Al	≥ 11	9.9 ± 0.3	1.86 ± 0.03	0.71 ± 0.07	0.4
Si+Au	≥ 19	18.9 ± 0.1	1.57 ± 0.09	0.64 ± 0.09	4.7
Au+Al	≥ 26	23.5 ± 0.2	2.07 ± 0.02	0.76 ± 0.02	6.6
Au+Au	≥ 78	72.0 ± 0.9	1.76 ± 0.01	0.69 ± 0.02	1.1

Table 1: Summary of gaussian fits of the angular distributions to the form $dE_T^{L+R}/d\eta = \rho \exp[-(\eta - \eta_{peak})^2/2\sigma_{rms}^2]$.

Preliminary results for the differential cross-section, $d\sigma/dE_T^{L+R}$, versus E_T^{L+R} are shown in Fig. 2a for Si+Al,Au at 14.6A GeV/c and for Au+Al,Au at 11.6A GeV/c. As is usual with this type of distribution, there is a large cross-section for peripheral reactions at the lowest E_T, followed by a "plateau" which becomes an exponential "tail" at the highest E_T. The energy scale associated with the tail is largest for the largest system, namely Au+Au, and smallest for the smallest system, Si+Al. The tail for Au+Al is approximately 40% higher than that for Si+Au; this will be discussed further below. The systematic error on the absolute energy scale is 10%.

An important point is that the *shapes* of the distributions in Fig. 2a are different. An attempt to reproduce the Au+Au spectrum by changing the energy scale for the Si+Al and Si+Au spectra is shown in Fig. 2b. The energy scaling factor used arises from the ratio of the available kinetic energy in the center of mass system of the Fireball Model. Thus the Si+Al E_T scale is shifted by the ratio Au+Au/Si+Al=586 GeV/97 GeV=6.1, and that of Si+Au is shifted by the ratio Au+Au/Si+Au=586 GeV/154 GeV=3.8. The rescaled Si+Al spectrum does not exhibit the long plateau of Au+Au and the slope on the tail is not as steep. The "knee" of the rescaled Si+Au curve occurs at too low of an energy and the slope of the tail is also not as steep as Au+Au. A better match between Si+Au and Au+Au is found for a scale factor of 4.5, but the tails still have different slopes. The failure of the energy rescaling picture to describe the projectile dependence from ^{28}Si to ^{197}Au is in contrast to its success in explaining the projectile dependence from ^{16}O to ^{28}Si at 14.6A GeV/c [2], as well as the dependence from ^{16}O to ^{32}S at 200A GeV [6].

The angular distributions, $dE_T^{L+R}/d\eta$, are shown in Fig. 3 versus the pseudorapidity, η. Only the more finely segmented right-side array was used in obtaining the distributions, and a cut has been used which keeps only central events on the tails defined by $d\sigma/dE_T^{L+R} \leq 10^{-2}$ barn/GeV. The specific cut thresholds are listed in Table 1, but the shapes of the $dE_T/d\eta$ distributions are not sensitive to the exact threshold values. The peaks of all four distributions are clearly within the detector acceptance, and the curves can be approximated by gaussians, as summarized in Table 1. For all four systems, the E_T measured inside the detector acceptance is about 60% of the E_T extrapolated over all pseudorapidity from the gaussian fit. In particular, the difference in the energy of the tail of Au+Al compared to Si+Au can not be explained solely by an effect of the detector acceptance at the level of more than 5%.

The difference in the energy of the Si+Au and Au+Al tails must instead be attributed to a change in the composition of the signal in the lead-glass, presumably from fast forward-

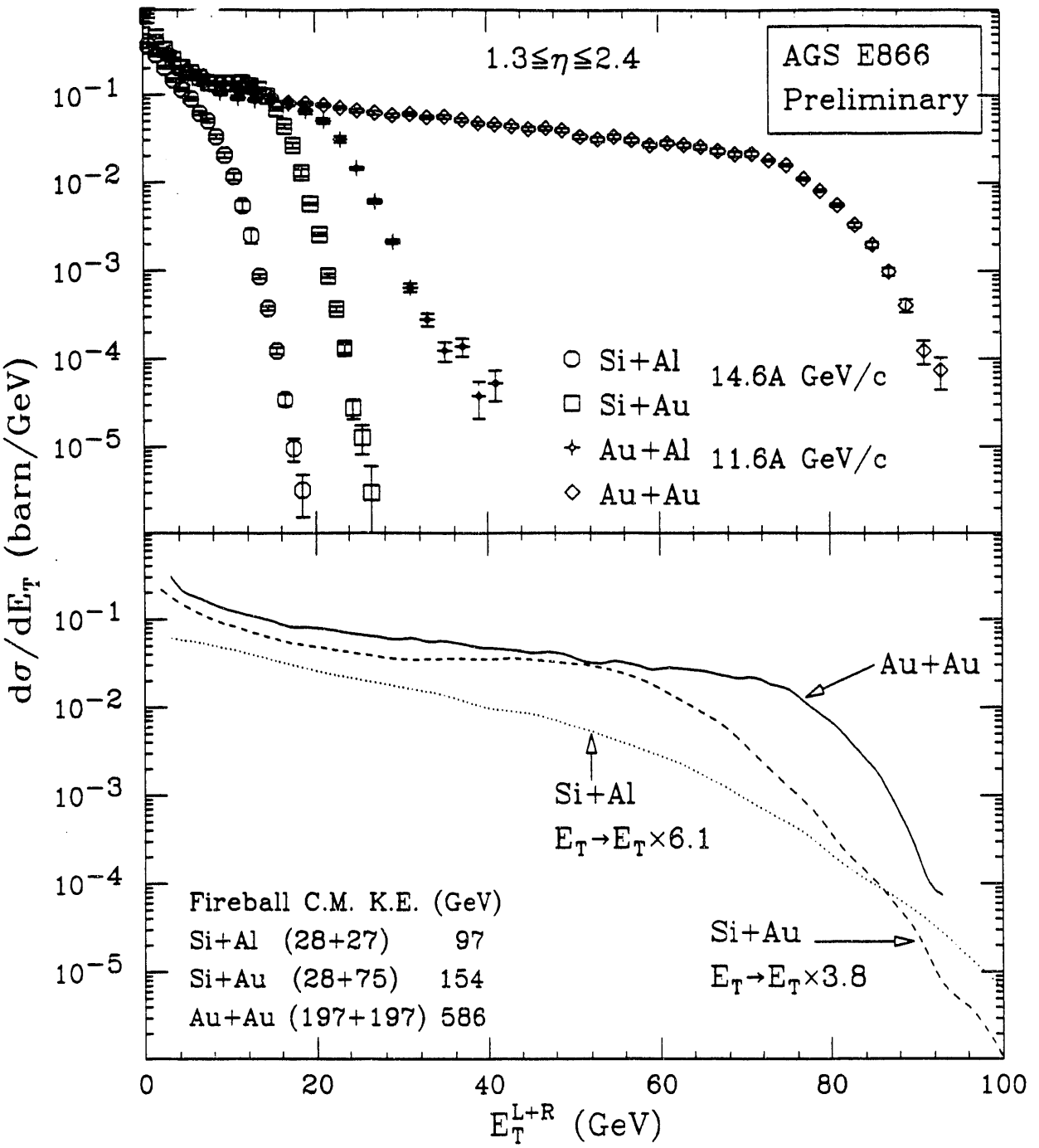

Fig. 2: a) The differential cross-section versus E_T^{L+R} for Si+Al,Au and Au+Al,Au. b) The Au+Au spectrum compared to those of Si+Al and Si+Au with a shift in the energy scale given by the ratio of available kinetic energy in the fireball center-of-mass system.

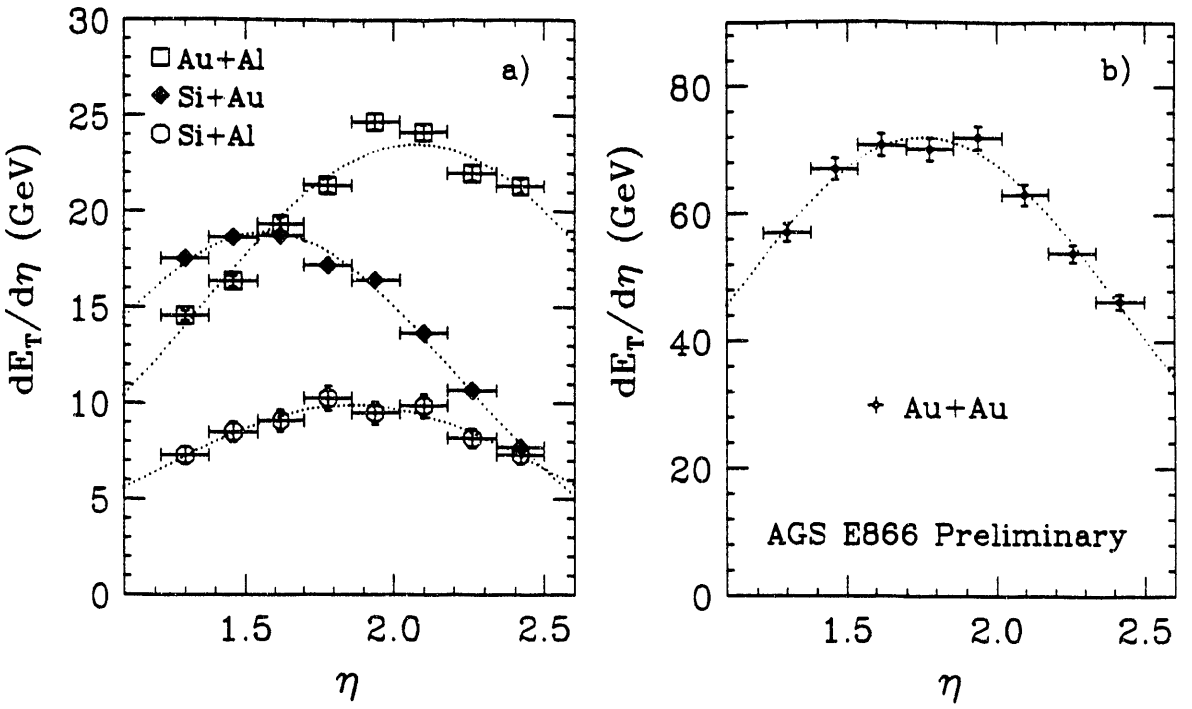

Fig. 3: The angular distribution $dE_T^{L+R}/d\eta$ for events on the tail: a) $E_T^{L+R} \geq 11$ GeV for Si+Al, $E_T^{L+R} \geq 19$ GeV for Si+Au, $E_T^{L+R} \geq 26$ GeV for Au+Al, and b) $E_T^{L+R} \geq 78$ GeV for Au+Au. The gaussian fits given in Table 1 are shown as dotted curves.

moving protons in Au+Al. (The equivalent protons in Si+Au will be below Čerenkov threshold in the laboratory frame.) This picture predicts proportionally more of the Au+Al signal deriving from higher pseudorapidities, but fails to explain why the Au+Au distribution is symmetric about $y_{NN} = 1.6$. Future measurements of the particle distributions in Au+A at midrapidity should settle the question of the signal composition.

5. Forward Energy Spectra

A different measure of the centrality of the collision comes from the forward kinetic energy of the projectile as detected in the ZCAL. Preliminary target-out corrected differential cross-sections versus the forward kinetic energy, T_{ZCAL}, are shown in Fig. 4 for Au+Au and Si+Al, both with a minimum bias trigger. The energy scale for Si+Al has been shifted up by the ratio of the initial beam kinetic energies, namely 2108 GeV/383 GeV = 5.5, in order to compare the shapes of the two spectra. It should be noted that the energy resolution of the ZCAL was about four times worse than that from previous runs[1] due to degradation of the scintillator in the calorimeter; this tended to broaden the peak at the beam energy but was not important for central events, i.e., those with the lowest T_{ZCAL}.

The difference in behavior for the two systems at the lowest relative T_{ZCAL} is striking. While the Au+Au spectrum falls from the beam energy peak to a long plateau which drops suddenly just before $T_{ZCAL} = 0$, the Si+Al falls from the beam energy peak more gradually and cuts off at a relatively higher T_{ZCAL}. For the most central 4% of the cross-section, the

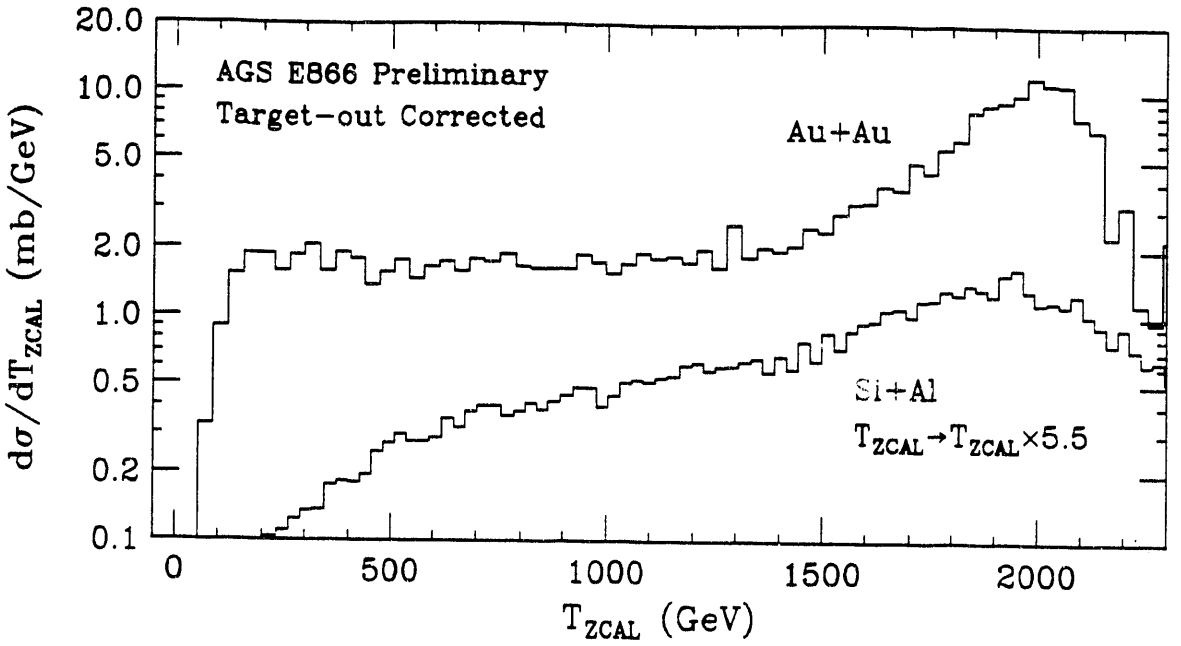

Fig. 4: The target-out corrected forward energy spectra for minimum bias Au+Au and Si+Al events as measured in the ZCAL. The energy scale on the Si+Al histogram has been shifted up by the ratio of the initial beam kinetic energies, namely 5.5.

mean fraction of projectile nucleons which are participants, defined as $1 - \langle T_{zcal} \rangle / T_{beam}$, is 91% for Au+Au and 83% for Si+Al.

6. Correlation Between Forward and Transverse Energy

The transverse and forward energies for Au+Au are plotted together in Fig. 5. A clear anticorrelation is observed with the contour curve definitely bending upward towards higher E_T^{L+R} for the lowest T_{ZCAL} (most central) events. Indeed, for $T_{ZCAL} < 283$ GeV, a condition which corresponds to 4% of the total cross-section and which has been used in an analysis of E866 spectrometer data[7], there is a wide range of E_T^{L+R} values covered. This suggests large fluctuations in the produced particle multiplicity for a given number of participants. A suggestion for future analysis of E866 data is to make a cut on both low T_{ZCAL} *and* high E_T^{L+R}. Such a "Grand Central Trigger" condition may choose events of interest for studying high density states of nuclear matter[8].

The upward turn in Fig. 5 is not a simple consequence of the geometry of Au+Au collisions. This may be seen by comparing to the Fritiof model[9] which allows for multiple projectile nucleon interactions while treating the individual projectile nucleon contributions independently. The predicted correlation plot of E_T^{L+R} and T_{ZCAL} is shown in Fig. 6a, where a linear relation is observed. Here the ZCAL response and treatment of projectile spectator nucleons follows Ref. 1, and the lead-glass signal from charged particles is assumed to be Čerenkov radiation with an equivalent signal energy[3] of 0.45 GeV gradually turning on above $\beta_c = 0.6$. (There is a $\pm 10\%$ systematic uncertainty in the *absolute* modelled E_T

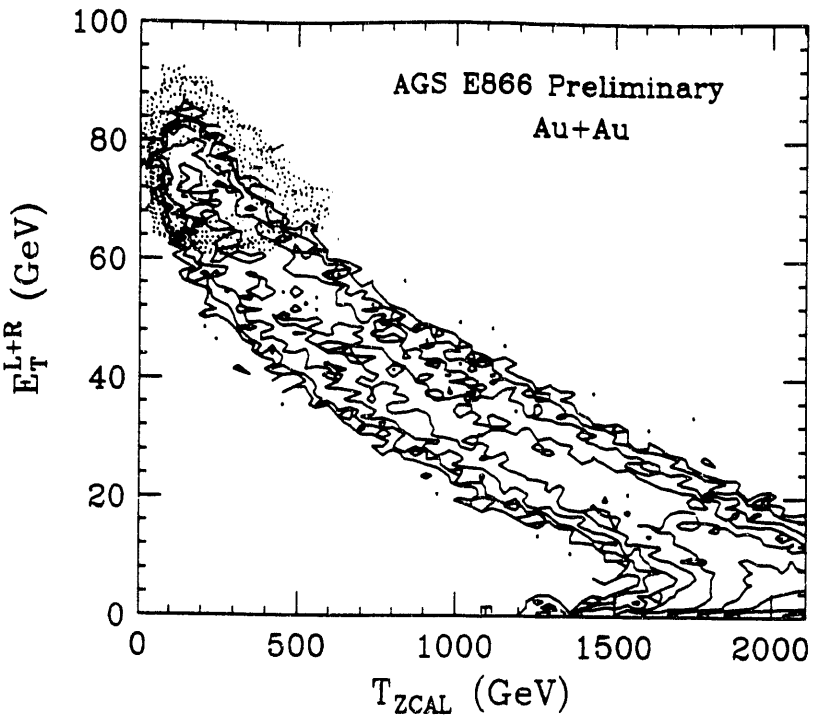

Fig. 5: Correlation plot of the transverse energy E_T^{L+R} versus forward energy T_{ZCAL} for Au+Au. Solid contours are from a minimum bias trigger and dotted contours are from a high E_T^{L+R} hardware trigger. The contour lines are logarithmic with a factor of two difference between adjacent lines.

scale reflecting uncertainty in the lead-glass response, but this does not affect the discussion here.)

In contrast to Fritiof, ARC[10] is a full relativistic cascade model which allows reinteractions between all particles involved in the collision. The transverse-forward energy correlation for ARC shown in Fig. 6b displays the curving up at low T_{ZCAL} seen in the data and missing from Fritiof. For the most central events, ARC predicts a baryon density at midrapidity of up to 9 times normal nuclear density, and it is there that the model may begin to break down[11].

7. Summary of Results

In conclusion, we have seen that the $d\sigma/dE_T$ spectral tails roughly behave as Au+Au/Si+Al =6 and Au+Au/Si+Au=4.5, but that the Au+Au spectrum has a different shape than those of Si+Al,Au. Unlike the case for O+A and Si+A, the projectile dependence can not be explained by simple energy rescaling. The Si+Au and Au+Al high-energy tails are not identical, but reflect the systematics of the detector response. When scaled by the appropriate beam energy, the forward energy spectrum of Au+Au has a longer plateau and relatively more cross-section near $T_{ZCAL} = 0$ than that for Si+Al, showing a somewhat greater ability of nucleons to become participants in the larger system. Finally, it was shown for the case of Au+Au that transverse and forward energies are anticorrelated, with the correlation plot curving upwards and giving a wide range of E_T for events at low T_{ZCAL}. This indicates

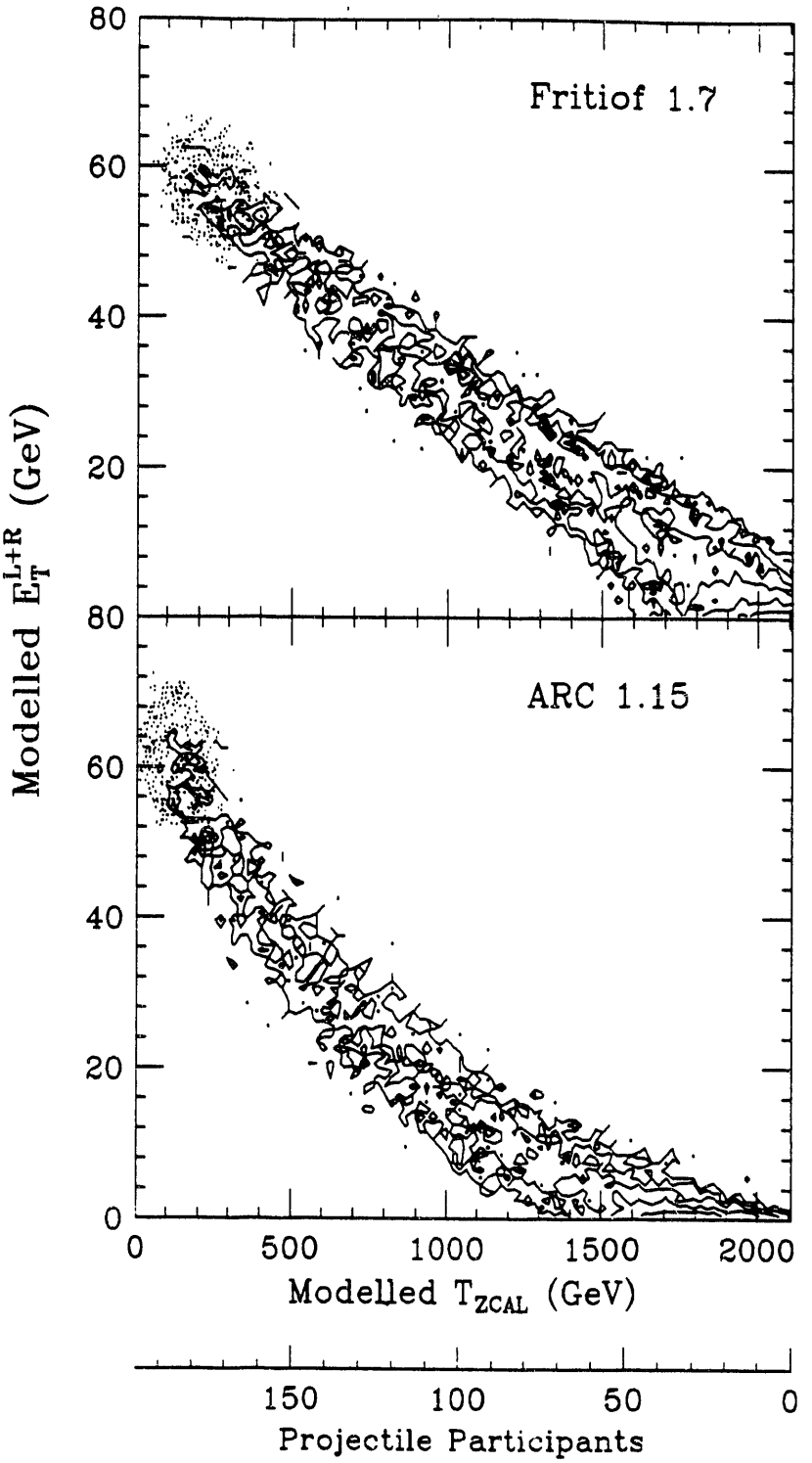

Fig. 6: Correlation contour plot of E_T^{L+R} versus T_{ZCAL} for Au+Au at 11.6A GeV/c based on the models a) Fritiof 1.7 with standard parameters, and b) ARC 1.15. Solid contours are from all impact parameters and dotted contours are from a run with $b < 2$ fm. Each contour level represents a factor of two. The projectile participant scale assumes a linear relation with T_{ZCAL}.

large fluctuations in particle production for central events with a given number of participants. The simple geometric picture provided by Fritiof can not reproduce these features qualitatively, but the full cascade model ARC, which predicts very high baryon density, can.

This set of calorimetry experiments provided a first glimpse at the Au+Au reactions, and as such are a valuable probe of the complex dynamics. Together with future results from the magnetic spectrometer, etc., a fuller understanding of baryon stopping and particle production will emerge.

8. Acknowledgements

The operations staffs of the BNL AGS, Booster and Tandem are gratefully acknowledged for providing the heavy ion beams. Tom Schlagel kindly provided a list of simulated events from the ARC model calculation.

Experiment 866 is supported by the U.S. Department of Energy contracts and grants with ANL, BNL, UC-Berkeley, UC-Riverside, Columbia, LLNL, and MIT, by NASA under contract with UC-Berkeley and by the US-Japan High Energy Physics Collaboration treaty.

9. References

1. T. Abbott *et al.*, Phys. Rev. **C44**, 1611 (1991).
2. T. Abbott *et al.*, Phys. Rev. **C45**, 2933 (1992).
3. Y. Akiba, Ph. D. thesis, INS-IM-6, University of Tokyo (1989).
4. M.J. Tannenbaum, in *Proc. of the Workshop on Heavy Ion Physics at the AGS*, O. Hansen, ed., BNL-44911, (National Technical Information Service, 1990) p. 45.
5. D. Beavis *et al.*, Nucl. Instrum. Methods **A281**, 367 (1989).
6. H.G. Ritter, Nucl. Phys. **A488**, 651c (1988).
7. M. Gonin *et al.*, Proc. Int. Nucl. Physics Conf., July 26-August 1, 1992, Wiesbaden, Germany (in press); also this volume.
8. R. Debbe and D. Roehrich, poster presented at Quark Matter '91 Conf., Nov. 11-15, 1991, Gatlinburg, TN, performed this type of analysis for Si+A data.
9. B. Nilsson-Almqvist and E. Stenlund, Comput. Phys. Commun. **43**, 387 (1987); B. Andersson, G. Gustafson and B. Nilsson-Almqvist, Nucl. Phys. **B281**, 289 (1987).
10. Y. Pang, T.J. Schlagel and S.H. Kahana, Phys. Rev. Lett. **68**, 2743 (1992).
11. Y. Pang, private communication (1992).

END

DATE
FILMED
6/30/93